

A correlation between the H I 21-cm absorption strength and impact parameter in external galaxies

S. J. Curran^{1*}, S. N. Reeves^{2,3,4}, J. R. Allison² and E. M. Sadler^{3,4}

¹*School of Chemical and Physical Sciences, Victoria University of Wellington, PO Box 600, Wellington 6140, New Zealand*

²*CSIRO Astronomy and Space Science, PO Box 76, Epping NSW 1710, Australia*

³*Sydney Institute for Astronomy, School of Physics, University of Sydney, NSW 2006, Australia*

⁴*ARC Centre of Excellence for All-sky Astrophysics (CAASTRO)*

Accepted —. Received —; in original form —

ABSTRACT

By combining the data from surveys for H I 21-cm absorption at various impact parameters in near-by galaxies, we report an anti-correlation between the 21-cm absorption strength (velocity integrated optical depth) and the impact parameter. Also, by combining the 21-cm absorption strength with that of the emission, giving the neutral hydrogen column density, N_{HI} , we find no evidence that the spin temperature of the gas (degenerate with the covering factor) varies significantly across the disk. This is consistent with the uniformity of spin temperature measured across the Galactic disk. Furthermore, comparison with the Galactic N_{HI} distribution suggests that intervening 21-cm absorption preferentially arises in disks of high inclinations (near face-on). We also investigate the hypothesis that 21-cm absorption is favourably detected towards compact radio sources. Although there is insufficient data to determine whether there is a higher detection rate towards quasar, rather than radio galaxy, sight-lines, the 21-cm detections intervene objects with a mean turnover frequency of $\langle \nu_{\text{TO}} \rangle \approx 5 \times 10^8$ Hz, compared to $\langle \nu_{\text{TO}} \rangle \approx 1 \times 10^8$ Hz for the non-detections. Since the turnover frequency is anti-correlated with radio source size, this does indicate a preferential bias for detection towards compact background radio sources.

Key words: galaxies: structure – galaxies: ISM – radio lines: galaxies – quasars: absorption lines

1 INTRODUCTION

Study of the cool neutral gas over various redshifts gives insight into the evolution of the star forming reservoir and is a science goal of the forthcoming Square Kilometre Array (SKA, Morganti et al. 2015). The distribution of cool neutral hydrogen (H I) with galactocentric radius in external galaxies is crucial in interpreting the data from the forthcoming surveys of H I 21-cm absorption with the SKA and its pathfinders.¹ To this end, we (Reeves et al. 2015, 2016) have undertaken a survey of 21-cm absorption of background radio sources at various impact parameters in the disks of intervening, nearby galaxies ($z < 0.04$, Fig. 1).

For impact parameters of $\rho \lesssim 20$ kpc, the H I detection rate is approximately 50 per-cent (Gupta et al. 2010; Borthakur et al. 2011, 2014; Srianand et al. 2013). However, Reeves et al. (2015) find a significantly lower detection rate (4 per-cent), which they attribute to the unbiased nature of their sample. That is, no target pre-

selection based upon impact parameter nor the nature of the background source. For a given sight-line, a background radio galaxy could result in a lower covering factor, reducing the observed optical depth in comparison to a quasar (see Sect. 2.2).

Although the gas density in a galaxy is known to decrease with galactocentric radius (e.g. Toomre 1963), none of the previous surveys have found convincing evidence of a decrease in 21-cm absorption strength with impact parameter (Gupta et al. 2010; Borthakur et al. 2011; Gupta et al. 2013; Zwaan et al. 2015). This is despite evidence of an anti-correlation between the Lyman- α and CIV equivalent widths and the impact parameter being well established in the optical/UV bands (e.g. Lanzetta et al. 1995; Tripp et al. 1998; Chen et al. 2001; Rao et al. 2011; Borthakur et al. 2015). By adding the latest results (Reeves et al. 2015, 2016; Dutta et al. 2016) to the previously published data and incorporating the limits, obtained from the non-detections, here we report the first clear evidence of an anti-correlation between the 21-cm absorption strength and the impact parameter.

* Stephen.Curran@vuw.ac.nz

¹ For example, the *First Large Absorption Survey in H I* (FLASH) on the Australian Square Kilometre Array Pathfinder (ASKAP), of which the *Boolarly Engineering Test Array* has already detected redshifted H I 21-cm (at $z = 0.44$, Allison et al. 2015).

Table 1. Summary of the searches for H I 21-cm absorption at various impact parameters in external galaxies. In the interest of consistency we quote the NED name of the galaxy, followed by its redshift. “Type” designates whether the search targeted quasar–galaxy pairs (P) or metal-line systems (M). For ease of matching, the sight-line is named as in the reference, followed by its NED classification – galaxy (G), QSO (Q) or unclassified radio source (U). This is followed by the velocity integrated optical depth (or the 3σ limit) of the 21-cm absorption, the impact parameter, the search reference and finally the blue and far-infrared luminosities as obtained from the photometry (see main text).

Galaxy (NED)	z_{gal}	Type	Sight-line	Class	N_{HI} [10^{20} cm^{-2}]	$\int \tau dv$ [km s^{-1}]	ρ [kpc]	Ref.	L_{B} [$\log_{10} \text{W Hz}^{-1}$]	L_{K}
CGCG 045–091	0.032465	P	134528.765+034720.09	Q	—	< 0.08	53.3	B11	21.54	22.42
CGCG 244–046	0.032092	P	125247.588+474042.81	U	—	< 0.06	18.1	B11	21.55	22.61
...	125249.326+474042.19	Q	—	< 0.10	15.2	B11
ESO 150–G005	0.004790	P	C-ESO150-G005-1	U	—	< 14.1	18.7	R15	20.60	—
...	...	P	C-ESO150-G005-2	U	—	< 23.3	25.1	R15
ESO 300–G014	0.003186	P	C-ESO300-G014-1	U	1.4 ± 0.1	< 1.22	11.6	R16	20.62	21.78
...	C-ESO300-G014-2	U	8.1 ± 0.2	< 1.63	6.1	R16
ESO 345–G046	0.007168	P	C-ESO345-G046	U	28 ± 12	< 2.90	13.6	R15	21.16	—
ESO 357–G012	0.005227	P	C-ESO357-G012-1a	U	1.0 ± 0.2	< 3.49	20.0	R16	20.82	21.69
...	C-ESO357-G012-1b	U	1.0 ± 0.2	< 11.7	18.8	R16
ESO 363-G015	0.004216	P	C-ESO363-G015-1	U	—	< 1.90	18.1	R16	20.77	19.28
...	C-ESO363-G015-2a	U	—	< 6.09	17.0	R16
...	C-ESO363-G015-2b	U	—	< 6.81	17.6	R16
ESO 400-G012	0.026999	M	2030–370	Q	2.7 ± 1.3	0.22	10.0	C92	21.48	21.79
ESO 402-G025	0.008577	P	C-ESO402-G025-1	U	5.2 ± 1.1	< 1.18	17.7	R15	20.46	20.57
...	...	P	C-ESO402-G025-2	U	9.3 ± 1.0	< 2.88	16.9	R15
ESO 576-G069	0.017809	M	1327–206	Q	0.6 ± 0.2	0.20	13.9	C92	21.48	22.24
IC 1914	0.003432	P	C-IC1914-1a	U	—	< 1.34	17.2	R16	20.63	19.76
...	C-IC1914-1b	U	—	< 1.91	16.9	R16
IC 1954	0.003542	P	C-IC1954	U	—	< 0.48	10.7	R15	20.50	21.40
IC 4386	0.006278	P	C-IC4386-1	U	—	< 0.97	21.5	R16	21.57	20.29
...	C-IC4386-2	U	3.2 ± 0.2	< 3.91	26.6	R16
IRAS 02483+4302	0.051440	M	0248+430	Q	—	0.26	15.0	H04	—	22.69
[KAC2002] A	0.437	M	1243–072	Q	—	0.75	11.6	K02	—	—
2MASX J08495751+5108416	0.312	M	J0849+5108	Q	—	0.95	14	G13	21.87	22.02
2MASX J13253523+4953246	0.047829	P	132534.240+495348.47	U	—	< 0.39	23.9	B11	21.12	22.20
...	132534.565+495342.26	Q	—	< 0.64	17.5	B11
2MASX J13540065+5650007	0.095513	M	4C +57.23	U	—	< 1.17	11	Z15	21.61	22.38
NGC 2188	0.002492	P	C-NGC2188-1a	G	1.5 ± 0.2	< 6.25	7.7	R16	20.93	20.21
...	C-NGC2188-1b	G	1.5 ± 0.2	< 8.37	8.0	R16
NGC 0628	0.002192	P	0131+154	Q	—	< 0.15	94.1	C90	21.18	21.54
NGC 0660	0.002835	P	0139+132	U	—	< 0.067	51.9	C90	20.17	21.96
NGC 1249	0.003576	P	C-NGC1249-1	U	2.9 ± 0.7	< 4.64	13.2	R16	21.18	20.67
...	C-NGC1249-2	U	—	< 5.28	19.6	R16
...	C-NGC1249-3a	U	—	< 9.54	25.0	R16
...	C-NGC1249-3b	U	—	< 10.5	25.5	R16
NGC 1566	0.005017	P	C-NGC1566-1	U	130 ± 19	< 3.30	17.2	R16	21.83	22.01
...	C-NGC1566-2a	U	6.6 ± 0.9	< 6.16	25.5	R16
...	C-NGC1566-2b	U	7.7 ± 0.9	< 13.42	21.7	R16
NGC 3067*	0.004923	M	0955+326	Q	0.8 ± 0.4	0.12	11.1	C92	21.18	21.48
NGC 4138	0.002962	P	3C 268.4	Q	—	< 0.08	10.5	H75	20.88	21.57
NGC 4651	0.002628	P	3C 275.1	Q	—	< 0.010	12.1	C90	21.21	21.60
NGC 5156	0.009967	P	C-NGC5156	U	14.3 ± 2.2	1.02	18.5	R16	22.15	22.43
NGC 5832	0.001491	P	3C 309.1	Q	1.0	< 0.014	11.2	H75	20.23	—
NGC 6503	0.000083	P	1749+70.1	Q	—	< 0.01	10.3	B88	20.80	20.71
NGC,7162A	0.007569	P	C-NGC7162A-1	U	4.4 ± 1.3	< 2.25	16.1	R16	21.22	—
...	C-NGC7162A-2	G	—	< 4.01	46.7	R16
NGC 7412	0.005704	P	C-NGC7412-1	U	6.6 ± 0.7	< 2.08	12.9	R15	21.46	21.48
...	C-NGC7412-2	U	6.6 ± 0.7	< 2.63	12.6	R15
NGC 7413*	0.032489	P	3C 455	Q	—	< 0.026	14.9	C90	21.84	22.53
NGC 7424	0.003132	P	C-NGC7424	Q	103 ± 14	< 0.99	10.0	R15	21.02	20.62
NGC 7490	0.020724	P	2304+32B	U	—	< 0.10	204.8	C90	—	22.53
PGC 016074	0.066046	P	0446–208C	Q	—	0.21	15.4	C92	—	—
...	0446–208E	Q	—	0.32	37.1	C92
...	0446–208W	Q	—	0.63	35.2	C92
SDSS J074842.58+173450.6	0.052822	P	074841.773+173456.82	Q	—	< 0.10	13.5	B11	21.18	22.15
...	074841.786+173512.20	U	—	< 0.19	25.1	B11
...	074842.084+173443.37	U	—	< 0.26	10.4	B11

Table 1. Continued

Galaxy (NED)	z_{gal}	Type	Sight-line	Class	N_{HI} [10^{20} cm^{-2}]	$\int \tau dv$ [km s^{-1}]	ρ [kpc]	Ref.	L_{B} [$\log_{10} \text{W Hz}^{-1}$]	L_{K}
SDSS J082153.75+503125.7	0.1835	P	J0821+5031	Q	—	< 0.38	15.9	G10	—	—
...	...	P	082153.833+503120.57	Q	—	< 0.16	16.0	B11
SDSS J084912.42+275740.4	0.1948	P	084914.282+275729.90	Q	—	< 0.02	86.7	B11	21.82	—
SDSS J084957.48+510842.3	0.073485	P	J0849+5108	Q	—	< 0.08	19.4	G10	21.87	22.02
SDSS J085519.04+575140.7	0.026003	M	GB6 J0855+5751	G	—	< 0.75	9.5	Z15	20.49	—
SDSS J102257.92+123439.1	0.1253	P	102258.415+123426.26	Q	—	< 0.03	33.1	B11	21.46	22.37
...	...	P	102258.552+123439.94	U	—	< 0.13	20.9	B11
SDSS J104257.74+074751.3	0.03321	M	J104257.74+074751.3	Q	—	0.19	1.7	B10	—	—
...	...	P	104257.598+074850.60	Q	—	0.04962	1.7	B11
SDSS J010643.94-103419.3	0.146	P	010644.15-103410.5	Q	—	< 0.02	23.4	B11	21.69	22.54
SDSS J110736.60+090114.7	1.22823	P	110736.607+090114.72	Q	—	< 0.18	8.1	B11	—	—
SDSS J111025.09+032138.8	0.030115	P	J1110+0321C	Q	—	< 2.8	11.2	G10	21.17	—
...	J1110+0321E	Q	—	< 0.13	22.5	G10
...	...	P	J1110+0321W	Q	—	< 0.08	15.3	G10
SDSS J124157.26+633237.6	0.143	P	J1241+6332C	Q	—	2.90	11.0	G10	—	22.49
...	J1241+6332E	Q	—	< 2.50	34.0	G10
...	J1241+6332W	Q	—	< 0.62	53.0	G10
SDSS J122847.72+370606.9	0.138336	P	J1228+3706	Q	—	< 0.07	15.0	G10	—	—
SDSS J132839.89+622136.0	0.0423	P	132840.599+622136.65	Q	—	< 0.04	4.2	B11	20.46	—
SDSS J141629.25+372120.4	0.0341	P	141631.039+372203.01	Q	0.17 [†]	< 0.16	32.4	B11	—	—
...	141630.672+372137.09	U	...	< 0.16	16.2	B14
SDSS J144304.53+021419.3	0.371503	M	J1443+0214	G	—	3.4	< 5	G13	21.75	—
SDSS J160659.13+271642.6	0.046199	P	160658.315+271705.86	Q	0.32 [†]	< 0.03	23.3	B11	20.95	—
SDSS J163956.38+112802.1	0.08	M	J163956+112758	G	—	15.7	4	S13	21.23	22.23
UG 00439	0.017669	P	UM 266 – L1	Q	1.77 ± 0.19 [†]	< 0.07	24.7	D16	21.75	22.06
...	UM 266 – C	...	—	—	24.8	D16
...	...	P	UM 266 – L2	...	—	0.08	25.7	D16
UGC 07408	0.001541	P	122105.480+454838.80	U	4.6 [†]	0.11	3.3	B11	19.80	20.63
...	122106.854+454852.16	Q	4.6 [†]	1.53	2.8	B14
...	122107.811+454908.02	Q	4.6 [†]	< 0.47	2.6	B14
UGC 12081	0.038817	P	2231+0953	Q	—	< 0.10	92.3	C90	—	22.80

References: H75 – Haschick & Burke (1975), B88 – Boisse et al. (1988), C90 – Corbelli & Schneider (1990), C92 – Carilli & van Gorkom (1992), K02 – Kanekar et al. (2002), H04 – Hwang & Chiou (2004), B10 – Borthakur et al. (2010), G10 – Gupta et al. (2010), B11 – Borthakur et al. (2011), G13 – Gupta et al. (2013), S13 – Srianand et al. (2013), B14 – Borthakur et al. (2014), R15 – Reeves et al. (2015), Z15 – Zwaan et al. (2015), D16 – Dutta et al. (2016), R16 – Reeves et al. (2016).

Notes: *Also observed by Haschick & Burke (1975). [†]Obtained from the quoted integrated flux density of the HI emission or the quoted HI mass.

2 DATA, RESULTS AND ANALYSIS

2.1 HI 21-cm absorption strength and impact parameter

2.1.1 Raw impact parameters

There are now 90 spectral line observations of radio source sight-lines through the disks of galaxies (summarised in Table 1). In order to fully utilise these data, we include the upper limits to the optical depths (from the non-detections), via the *Astronomy SURVival Analysis* (ASURV) package (Isobe et al. 1986). These are added to the 16 detected sight-lines as censored data points. For the bivariate data, a generalised non-parametric Kendall-tau test gives a probability of $P(\tau) = 9.39 \times 10^{-4}$ of the observed $\int \tau dv$ - ρ anti-correlation arising by chance, which is significant at $S(\tau) = 3.31\sigma$, assuming Gaussian statistics (Fig. 2, top panel).

As seen from Table 1, only 14 of the 90 sight-lines were originally targeted as known metal-line absorbers, although these drive the correlation giving a $S(\tau) = 1.94\sigma$ significance from just 14 data points. However, this is due to the metal-line absorbers constituting 11 of the 16 detections, which define the parent population against which the limits are quantified, thus requiring their inclusion.

The limits may also be included in the binned univariate data to give the mean $\int \tau dv$ value of each bin, via the Kaplan–Meier estimator which gives a maximum-likelihood estimate based upon the parent population (Feigelson & Nelson 1985). Presenting the data thus, it is visually apparent that the absorption strength does decrease with increasing impact parameter (Fig. 2, bottom panel).

In addition to the generalised Kendall-tau test and the Kaplan–Meier estimates, we split the data in half via the median impact parameter: At $\rho < 16.2$ kpc, there are 14 detections and 31 non-detections, that is a 31.1 per-cent detection rate. Applying this to the $\rho > 16.2$ kpc bin, gives a binomial probability of 1.16×10^{-5} of obtaining two detections or fewer out of 45 sight-lines, which is significant at 4.37σ .

2.1.2 Normalised impact parameters

Although by the inclusion of the limits, we see a decrease in absorption strength with impact parameter, the sample is heterogeneous, comprising a variety of background source classifications (discussed in Sect. 2.2), in addition to potential differences in the foreground absorbing galaxies. These may arise from the search strategy of each individual survey, whether an unbiased survey to-

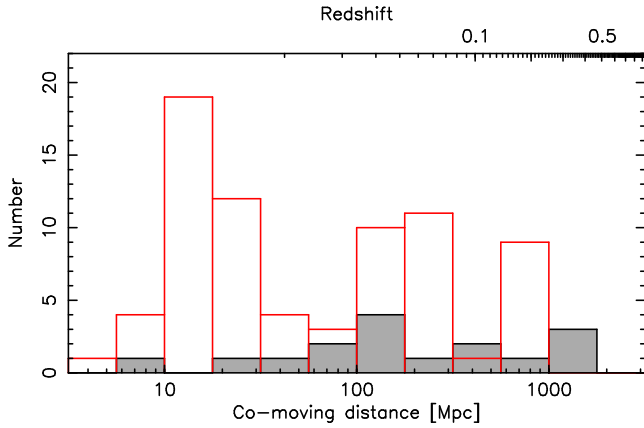


Figure 1. The redshift distribution of the galaxies searched for H I 21-cm at various impact parameters. The filled histogram shows the 21-cm detections and the unfilled the non-detections. The galaxies of Reeves et al. (2015, 2016) are selected from the H I Parkes All-Sky Survey (HIPASS, Koribalski et al. 2004) and so have redshifts of $z < 0.04$.

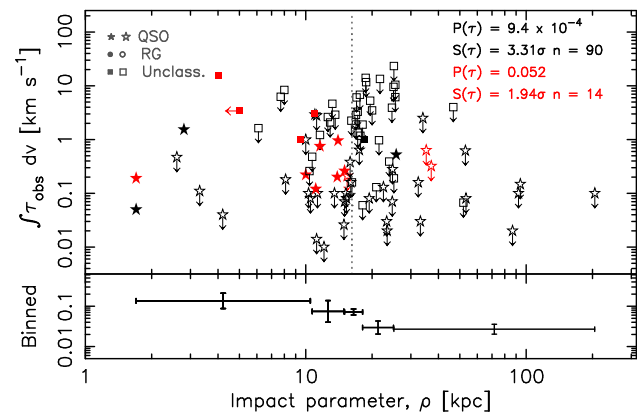


Figure 2. The velocity integrated optical depth versus the impact parameter for all of the published searches. The shapes show the classification of the background source: star – quasar/Quasi-Stellar Object (QSO), circle – Radio Galaxy (RG) and square – unclassified radio source, with the coloured symbols representing the known metal-line absorbers. The downward arrows signify the 3σ upper limits and the dotted vertical line shows where the sample is split in half with 45 sight-lines each at $\rho < 16.2$ kpc and $\rho > 16.2$ kpc. The probability of the correlation arising by chance, $P(\tau)$, and the corresponding significance, $S(\tau)$, is shown in the top right for both the whole sample (black text) and the known metal-line absorbers only (coloured text). The bottom panel shows the binned values, including the limits via the Kaplan–Meier estimator, in equally sized bins. The horizontal error bars show the range of points in the bin and the vertical error bars the 1σ uncertainty in the mean value

towards galaxy–quasar pairs or the selection of *known* metal-line absorbers.² The detection rate of the former is just 7%, compared to 79 per-cent for the latter, with these also tending to be at low impact parameters (Fig. 2). Such metal-line absorbers also comprise the foreground galaxies in the optical surveys which exhibit an equivalent width–impact parameter anticorrelation (Sect. 1).

² Although this does not preclude any of the 76 designated as pairs as being potentially metal-rich – 11 have been detected in Ca II absorption (see Carilli & van Gorkom 1992; Hwang & Chiou 2004; Gupta et al. 2010), although a further nine have been searched and not detected (see Corbelli & Schneider 1990; Borthakur et al. 2010; Gupta et al. 2010).

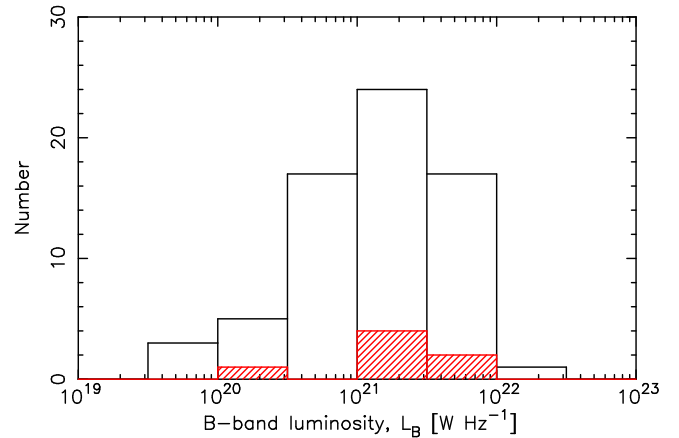


Figure 3. The distribution of the blue-band luminosities of the absorbing galaxies, where sufficient photometry is available. The hatched histogram shows the metal-line searches and the unfilled the galaxy–quasar pair searches.

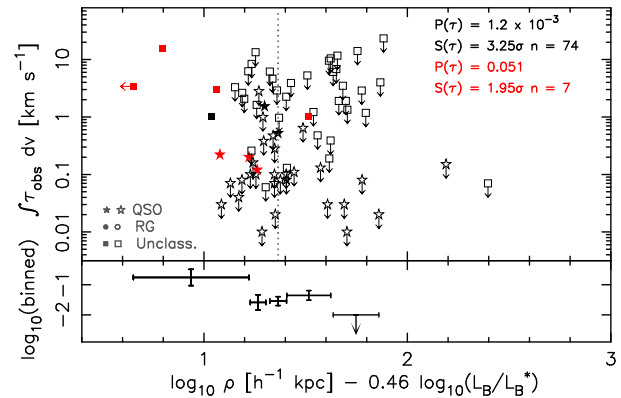


Figure 4. As Fig. 2 but with the impact parameter normalised by the B-band luminosity (cf. Chen et al. 2001).

Until all of the sample is observed and their metallicities quantified, this possible bias cannot be directly removed. However, both metallicity and equivalent width appear to be correlated with galaxy size (Ellison 2006; Curran et al. 2007; Murphy et al. 2007) and so a potentially wide range of metallicities is expected to reflect a large range of galaxy sizes. This could have the effect of a given impact parameter, which lies well within the disk for an L^* (high metallicity) galaxy, being located well outside the disk of a dwarf galaxy. In order to account for this, we normalise each impact parameter by the luminosity of the galaxy: As described in Curran et al. (2013b), for each galaxy we obtain the photometry from NASA/IPAC Extragalactic Database (NED), the Wide-Field Infrared Survey Explorer (WISE) and the Two Micron All Sky Survey (2MASS), correcting each value for Galactic extinction (Wilhelm 2013) before fitting to the required wavelength in the galaxy rest-frame.

We summarise the derived blue-band luminosities in Fig. 3. Using these to normalise the impact parameter, via the same $(\rho/h) \times (L_B/L_B^*)^{-0.46}$ correction as Chen et al. (2001), we find the absorption strength–impact parameter anti-correlation retains a similar significance, although with 16 fewer data points. As before, we can also compare detection rates above and below the median (normalised) impact parameter: At $(\rho/h) \times (L_B/L_B^*)^{-0.46} < 18.7$ kpc, there are 9 detections and 28 non-detections, that is a 24.3 per-cent detection rate. Applying this to the > 18.7 kpc bin, gives a

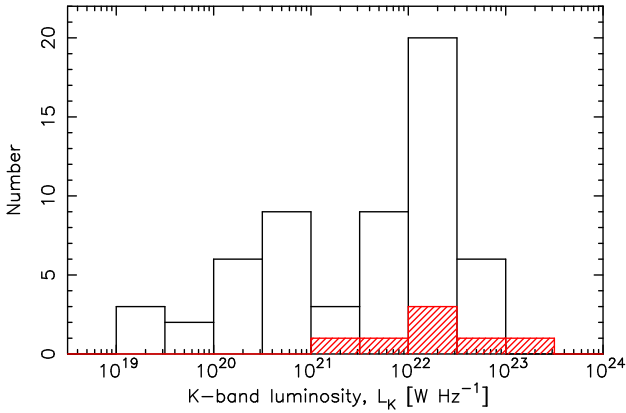


Figure 5. As Fig. 3, but for the near-infrared luminosity.

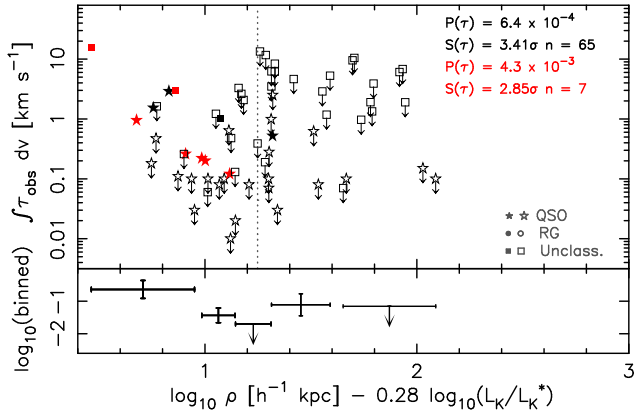


Figure 6. As Fig. 4 but with the impact parameter normalised by the K-band luminosity (cf. Chen et al. 2001).

binomial probability of 4.28×10^{-4} of obtaining two or fewer detections out of 37 sight-lines, which is significant at 3.52σ .

Chen et al. (2001) also normalise the impact parameter by the near-infrared luminosity, since this is less susceptible to extinction and irregularities caused by star formation, providing a better tracer of the total stellar mass. Normalising the impact parameter, the significance of the anti-correlation increases (Fig. 5) and, again comparing detection rates above and below the median (normalised) impact parameter: At $(\rho/h) \times (L_K/L_K^*)^{-0.28} < 22.2$ kpc, there are 10 detections and 21 non-detections, that is a 30.5 per-cent detection rate. Applying this to the > 22.2 kpc bin, gives a binomial probability of 3.05×10^{-5} of obtaining one detection or fewer out of 33 sight-lines, which is significant at 4.17σ .

Since we have both the blue and near-infrared luminosities for many of the galaxies, we can verify that the observed decrease in $\int \tau dv$ with impact parameter is not dominated by a colour bias, where the redder (and presumably, dustier) galaxies are more hospitable to the presence of cool gas.³ In Fig. 7 we plot the 21-cm absorption strength against the $B - K$ colour, where no correlation is apparent, leaving the decrease in gas density with impact parameter the major most likely cause. We also note that the known metal-line systems do exhibit some reddening ($B - K > 0$), which is consistent with the metallicity–dust (and molecular fraction) relation (see Curran et al. 2004 and references therein).

³ As is seen for both HI (Curran & Whiting 2010) and H₂ (Curran et al. 2011) at high redshift.

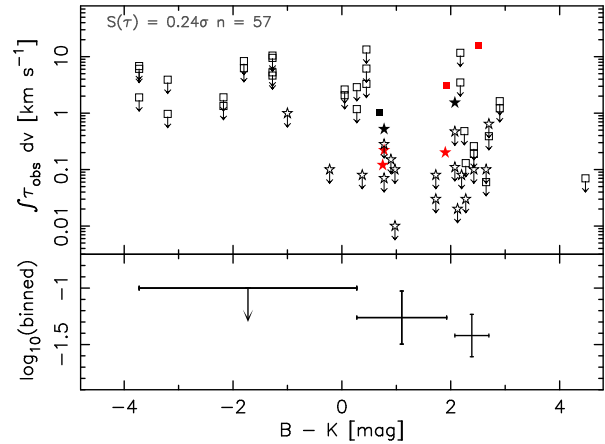


Figure 7. The velocity integrated optical depth versus the blue–near-infrared colours of the sample.

2.2 The effect of the background source size

As mentioned in Sect. 1, in addition to the impact parameter, it is believed that the extent of the background source can have an effect on the 21-cm detection rate. Specifically, for a given absorption cross section⁴ different background source sizes will have different observed optical depths, τ_{obs} , according to

$$\tau \equiv -\ln\left(1 - \frac{\tau_{\text{obs}}}{f}\right) \approx \frac{\tau_{\text{obs}}}{f} \text{ for } \tau_{\text{obs}} \lesssim 0.3 \Rightarrow \tau_{\text{obs}} \approx f\tau, \quad (1)$$

in the optically thin regime⁵, where the observed optical depth is defined as the ratio of the line depth to the continuum ($\tau_{\text{obs}} \equiv \Delta S/S$). Given that the covering factor ranges over $0 \leq f \leq 1$ for zero to full coverage of the background flux, larger background sources could give systematically lower observed optical depths. That is, we may expect the more compact quasar sight-lines to give a higher detection rate than those of radio galaxies.⁶

Addressing this, from the NED classifications, contrary to our expectations, we find a higher (50 – 100 per-cent) detection rate towards radio galaxies compared to the quasars (20 – 37 per-cent, Fig. 8). Performing a Pearson χ^2 -statistic test and applying Yates’s correction for continuity gives a significance of $p = 0.25$. Thus, the null hypothesis that the detection rates are the equal for radio galaxies and quasars cannot be rejected.

It is generally accepted that the turnover frequency of a radio source is anti-correlated with its extent (e.g. Fanti et al. 1990), with flat spectral indices arising from radio emission projected along our line-of-sight, thus also appearing more compact. Therefore, in the absence of high resolution radio images, we can use any clustering of either or both the turnover frequency/spectral index to gauge whether an unclassified background source is likely to be a quasar or a radio galaxy. We therefore compiled the photometry of each background source and, using the methods described

⁴ HI 21-cm absorbing clouds in external galaxies are believed to have 1.4 GHz cross-sections of ~ 100 pc (Braun 2012; Curran et al. 2013a).

⁵ The maximum of the sample is $\tau_{\text{obs}} = 0.24$ (Zwaan et al. 2015).

⁶ Curran et al. (2013a) have shown that the observed anti-correlation between the atomic hydrogen column density and the projected linear size of the background radio emission (Pihlström et al. 2003; Gupta & Saikia 2006a,b; Gupta et al. 2006; Orienti et al. 2006; Chandola et al. 2011) is most likely driven by the observed optical depth resulting from the coverage of the radio source.

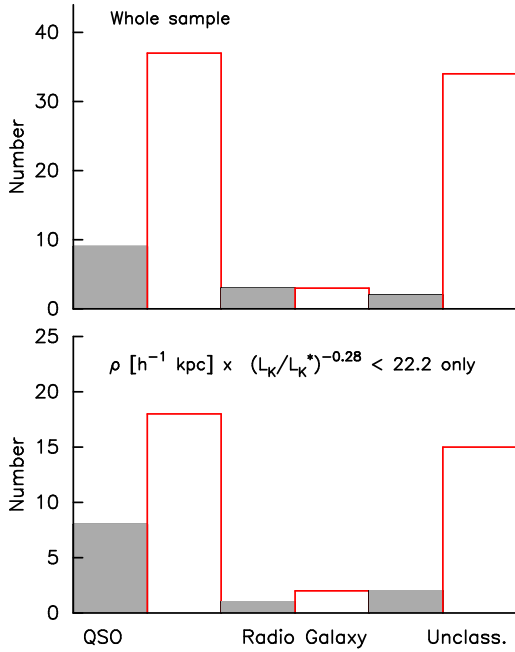


Figure 8. Breakdown of the various sight-line types, from NED (where quasars are classified as QSOs), for the whole sample (top panel) and for impact parameters less than the median value (bottom). The filled histogram shows the 21-cm detections and the unfilled the non-detections.

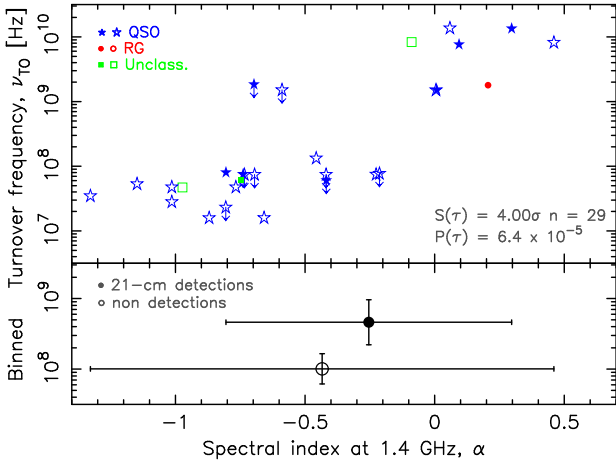


Figure 9. The rest-frame turnover frequency versus the spectral index for the background sources for which these could be determined. If no turnover is apparent in the radio SED we assume that this occurs below the lowest observed frequency (typically ~ 10 MHz) and use this to assign an upper limit to ν_{TO} . Again, the filled symbols represent the detections and the unfilled the non-detections with shapes representing the classification of the background source. In the bottom panel, the binned values of the detections and non-detections are shown.

in Curran et al. (2013b), determined the rest-frame turnover frequency, ν_{TO} , and spectral index at a rest frequency of 1.4 GHz, α .

From this (Fig. 9), we see that both the radio galaxies and unclassified sources, for which both ν_{TO} and α could be determined, are too few in number to exhibit any clustering, which is absent from the sources classified as QSOs in any case. Thus, at least at present, this method is of little use in predicting the nature of the background source. Based upon this limited sample,

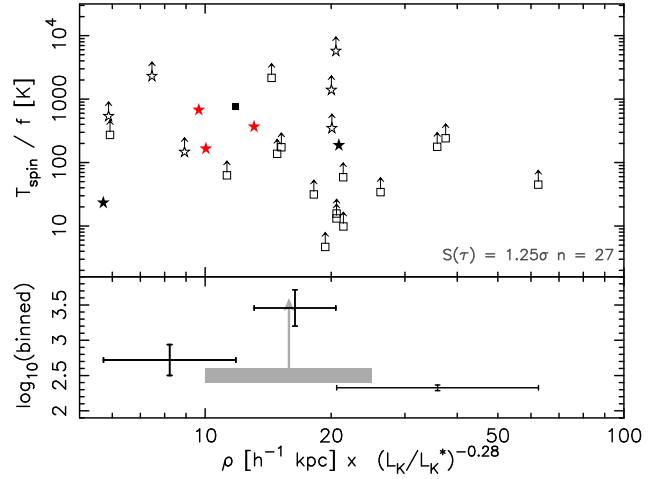


Figure 10. The spin temperature–covering factor degeneracy versus the normalized impact parameter for all of the published searches where a measure of the column density is available. In the top panel, the symbols are as per Fig. 2 and in the bottom panel the grey box shows the range in the outer Milky Way ($T_{\text{spin}} = 250 - 400$ K, Dickey et al. 2009). Since $f \leq 1$, this places a lower limit on T_{spin}/f .

however, we see that, while there is a large overlap in the spectral indices (although the detections are more “flat”, $|\alpha| < 0.5$), the detections and non-detections have distinct mean turnover frequencies ($\nu_{\text{TO}} = 10^{8.66 \pm 0.32}$ and $10^{8.00 \pm 0.21}$ Hz, respectively). Since the turnover frequency is anti-correlated with the source size (e.g. O’Dea 1998; Fanti 2000; Orienti et al. 2006), this is consistent with a detection bias towards the more compact radio sources, indicating that the covering factor is important.

2.3 Spin temperature and impact parameter

In the optically thin regime (Equ. 1), the neutral hydrogen column density, N_{HI} [cm^{-2}], is related to the absorption strength via

$$N_{\text{HI}} \approx 1.8 \times 10^{18} \frac{T_{\text{spin}}}{f} \int \tau_{\text{obs}} dv, \quad (2)$$

where T_{spin} [K] is the spin temperature of the gas and $\int \tau_{\text{obs}} dv$ [km s^{-1}] the velocity integrated optical depth of the absorption. The comparison of $\int \tau_{\text{obs}} dv$ with N_{HI} , from Lyman- α ($\lambda = 1216$ Å) observations, has shown an increase in T_{spin}/f with redshift, possibly suggesting an evolution in the spin temperature (e.g. Kanekar et al. 2014). However, the effect can adequately be accounted for by a decrease in f with redshift, due to the geometry effects of an expanding Universe (Curran 2012).

For this near-by sample we have the opportunity to determine whether T_{spin}/f generally varies with galactocentric radius, which could possibly introduce a beam-filling effect, where the mean value of T_{spin}/f within the beam could also contribute to a redshift dependence. Given that the gas is optically thin, for the low redshifts of the sample (Fig. 1), where 21-cm emission can be detected ($z \lesssim 0.2$, Catinella & Cortese 2015), the column density can be obtained directly from the brightness temperature of the line emission, T_{b} [K], via

$$N_{\text{HI}} \approx 1.8 \times 10^{18} \int T_{\text{b}} dv, \quad (3)$$

which in conjunction with Equ. 2 yields T_{spin}/f . Plotting this (Fig. 10), we see no evidence of a variation in T_{spin}/f with the nor-

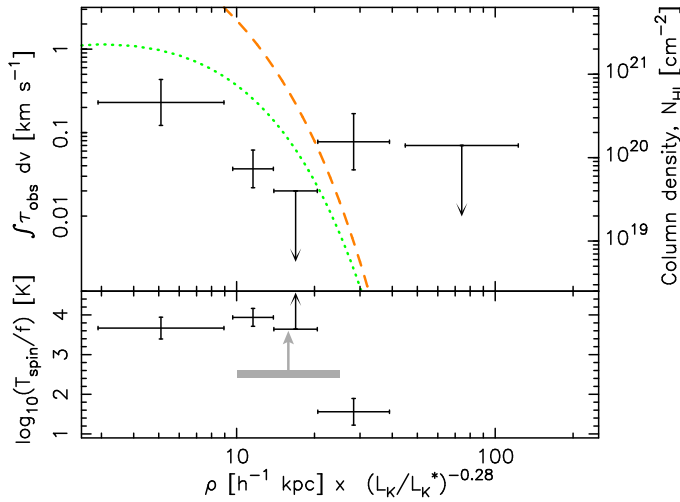


Figure 11. Top: The binned 21-cm absorption strength (left ordinate axis, Fig. 2) versus the impact parameter overlaid with the Galactic HI column density distribution (where $n_0 = 13.4 \text{ cm}^{-3}$, $R = 3 \text{ kpc}$ & $f_{\text{FL}} = 20$, right ordinate axis, dotted curve – viewed face-on, broken curve – viewed edge-on). Bottom: The values of T_{spin}/f obtained from the face-on case. As per Fig. 10, the grey box shows the range in the outer Milky Way.

malised impact parameter over $(\rho/h) \times (L_K/L_K^*)^{-0.28} \lesssim 100 \text{ kpc}$, which corresponds to the inner $r \approx 30 \text{ kpc}$ of galactocentric radius.

This is consistent the result of Dickey et al. (2009), who find remarkably little variation in the spin temperature over radii of 8–25 kpc in the Milky Way, despite both the 21-cm emission and absorption strengths varying by two orders of magnitudes.

2.4 Disk inclination

By assuming the known HI column density distribution of the Milky Way, we can estimate the approximate orientation of the average HI absorbing disk, based upon the $\int \tau dv - \rho$ relationship: The Galactic volume density of the neutral gas exhibits an exponential decrease with galactocentric radius according to $n = n_0 e^{-r/R}$, where $n_0 = 13.4 \text{ cm}^{-3}$ and the scale-length $R = 3 \text{ kpc}$ (Kalberla et al. 2007). The column density at each value of ρ is obtained from the volume density via $N_{\text{HI}} \equiv \int n dl$, where $N_{\text{HI}} = n h = n_0 e^{-\rho/R} h$ for a face-on ($i = 90^\circ$) disk⁷ and $N_{\text{HI}} = n_0 \int_0^\rho e^{-r/R} dr = n_0 R e^{-\rho/R}$ for an edge-on ($i = 0^\circ$) disk (Fig. 11).

From this, the face-on galactic disk appears to better trace the binned integrated optical depth values, again with $T_{\text{spin}}/f \sim 10^3 \text{ K}$ remaining approximately consistent with galactocentric radius out to $(\rho/h) \times (L_K/L_K^*)^{-0.28} \sim 20 \text{ kpc}$, beyond which this falls to $T_{\text{spin}}/f = 40 \text{ K}$ (Fig. 10). Applying the edge-on Galactic disk would give much larger values of T_{spin}/f , due either to very high spin temperatures and/or very low covering factors, the latter of which would be expected from a low inclination disk presenting a much smaller absorbing cross-section. We thus suggest that the targetted galaxies tend to have face-on inclinations, which is consistent with the observations of Reeves et al. (2015), who, from the azimuthal profiles of the HI emission, suggest that the intervening galaxies could be highly inclined (or highly asymmetric).

⁷ Where the height of the disk, h , is given by the flare factor, $f_{\text{FL}} = \rho/h$, which describes the flaring of the HI gas with galactocentric radius (Kalberla et al. 2007).

3 CONCLUSIONS

One of the goals of current surveys for HI 21-cm absorption at various impact parameters is to determine the expected detection rate of cool, neutral gas in distant galaxies with the next generation of large radio telescopes. An important aspect of this is the determination of the expected detection rate of 21-cm absorption at redshifts where the detection of 21-cm emission will not be possible. Here we demonstrate a clear anti-correlation between the integrated optical depth and the impact parameter, where previously only weak correlations were apparent at best (significance levels of $\leq 0.81\sigma$, Gupta et al. 2010; Borthakur et al. 2011; Gupta et al. 2013; Zwaan et al. 2015).

Also, investigating the hypothesis that 21-cm absorption is more readily detected towards quasars in comparison to radio galaxies, we find that the statistics are insufficient to draw any conclusions. However, we do find that the mean detection occurs towards a radio source with a higher turnover frequency than a non-detection. Since the turnover frequency is anti-correlated with source size, this suggests that the coverage of the background emission is important and thus we would expect a higher detection rate towards quasars in comparison to radio galaxies.

Lastly, using the neutral hydrogen column density obtained from the 21-cm emission, we find no statistical evidence for a variation of the spin temperature (degenerate with the covering factor) over the inner $\approx 30 \text{ kpc}$ of the disk, similar to the consistency in spin temperature observed across the Milky Way (Dickey et al. 2009). By using N_{HI} obtained from the HI distribution of the Milky Way, the observed $\int \tau dv - \rho$ correlation may suggest that the intervening galactic disks have high inclinations (close to face-on). This is consistent with the HI emission maps of Reeves et al. (2015), who suggest that galaxies which intercept background sources may be highly inclined.

ACKNOWLEDGEMENTS

We wish to thank the anonymous referee for their helpful and detailed comments and the *Radio Galaxy Morning Tea* group at the University of Sydney for useful discussion. This research has made use of the NASA/IPAC Extragalactic Database (NED) which is operated by the Jet Propulsion Laboratory, California Institute of Technology, under contract with the National Aeronautics and Space Administration and NASA’s Astrophysics Data System Bibliographic Service. This research has also made use of NASA’s Astrophysics Data System Bibliographic Service and ASURV Rev 1.2 (Lavalley et al. 1992), which implements the methods presented in Isobe et al. (1986).

REFERENCES

- Allison J. R. et al., 2015, MNRAS, 453, 1249
- Boisse P., Dickey J. M., Kazes I., Bergeron J., 1988, A&A, 191, 193
- Borthakur S. et al., 2015, ApJ, 813, 46
- Borthakur S., Momjian E., Heckman T. M., York D. G., Bowen D. V., Yun M. S., Tripp T. M., 2014, ApJ, 98
- Borthakur S., Tripp T. M., Yun M. S., Bowen D. V., Meiring J. D., York D. G., Momjian E., 2011, ApJ, 727, 52
- Borthakur S., Tripp T. M., Yun M. S., Momjian E., Meiring J. D., Bowen D. V., York D. G., 2010, ApJ, 713, 131
- Braun R., 2012, ApJ, 87, 749

- Carilli C. L., van Gorkom J. H., 1992, *ApJ*, 399, 373
- Catinella B., Cortese L., 2015, *MNRAS*, 446, 3526
- Chandola Y., Sirothia S. K., Saikia D. J., 2011, *MNRAS*, 418, 1787
- Chen H.-W., Lanzetta K. M., Webb J. K., Barcons X., 2001, *ApJ*, 559, 654
- Corbelli E., Schneider S. E., 1990, *ApJ*, 356, 14
- Curran S. J., 2012, *ApJ*, 748, L18
- Curran S. J., Allison J. R., Glowacki M., Whiting M. T., Sadler E. M., 2013a, *MNRAS*, 431, 3408
- Curran S. J., Tzanavaris P., Pihlström Y. M., Webb J. K., 2007, *MNRAS*, 382, 1331
- Curran S. J., Webb J. K., Murphy M. T., Carswell R. F., 2004, *MNRAS*, 351, L24
- Curran S. J., Whiting M. T., 2010, *ApJ*, 712, 303
- Curran S. J. et al., 2011, *MNRAS*, 416, 2143
- Curran S. J., Whiting M. T., Sadler E. M., Bignell C., 2013b, *MNRAS*, 428, 2053
- Dickey J. M., Strasser S., Gaensler B. M., Haverkorn M., Kavars D., McClure-Griffiths N. M., Stil J., Taylor A. R., 2009, *ApJ*, 693, 1250
- Dutta R., Gupta N., Srianand R., O’Meara J. M., 2016, *MNRAS*, 456, 4209
- Ellison S. L., 2006, *MNRAS*, 368, 335
- Fanti C., 2000, in *EVN Symposium 2000, Proceedings of the 5th European VLBI Network Symposium*, Conway J. E., Polatidis A. G., Booth R. S., Pihlström Y. M., eds., Onsala Space Observatory, Chalmers Technical University, Göteborg, Sweden, p. 73
- Fanti R., Fanti C., Schilizzi R. T., Spencer R. E., Nan Rendong, Parma P., van Breugel W. J. M., Venturi T., 1990, *A&A*, 231, 333
- Feigelson E. D., Nelson P. I., 1985, *ApJ*, 293, 192
- Gupta N., Saikia D. J., 2006a, *MNRAS*, 370, L80
- Gupta N., Saikia D. J., 2006b, *MNRAS*, 370, 738
- Gupta N., Salter C. J., Saikia D. J., Ghosh T., Jeyakumar S., 2006, *MNRAS*, 373, 972
- Gupta N., Srianand R., Bowen D. V., York D. G., Wadadekar Y., 2010, *MNRAS*, 408, 849
- Gupta N., Srianand R., Noterdaeme P., Petitjean P., Muzahid S., 2013, *A&A*, 558, A84
- Haschick A. D., Burke B. F., 1975, *ApJ*, 200, L137
- Hwang C.-Y., Chiou S.-H., 2004, *ApJ*, 600, 52
- Isobe T., Feigelson E., Nelson P., 1986, *ApJ*, 306, 490
- Kalberla P. M. W., Dedes L., Kerp J., Haud U., 2007, *A&A*, 469, 511
- Kanekar N., Athreya R. M., Chengalur J. N., 2002, *A&A*, 382, 838
- Kanekar N. et al., 2014, *MNRAS*, 438, 2131
- Koribalski B. S. et al., 2004, *AJ*, 128, 16
- Lanzetta K. M., Bowen D. V., Tytler D., Webb J. K., 1995, *ApJ*, 442, 538
- Lavalley M. P., Isobe T., Feigelson E. D., 1992, in *BAAS*, Vol. 24, pp. 839–840
- Morganti R., Sadler E. M., Curran S., 2015, *Advancing Astrophysics with the Square Kilometre Array (AASKA14)*, 134
- Murphy M. T., Curran S. J., Webb J. K., Ménager H., Zych B. J., 2007, *MNRAS*, 376, 673
- O’Dea C. P., 1998, *PASP*, 110, 493
- Orienti M., Morganti R., Dallacasa D., 2006, *A&A*, 457, 531
- Pihlström Y. M., Conway J. E., Vermeulen R. C., 2003, *A&A*, 404, 871
- Rao S. M., Belfort-Mihalyi M., Turnshek D. A., Monier E. M., Nestor D. B., Quider A., 2011, *MNRAS*, 416, 1215
- Reeves S. N., Sadler E. M., Allison J. R., Koribalski B. S., Curran S. J., Pracy M. B., 2015, *MNRAS*, 450, 926
- Reeves S. N., Sadler E. M., Allison J. R., Koribalski B. S., Curran S. J., Pracy M. B., 2016, *MNRAS*, 457, 2613
- Srianand R., Gupta N., Rahmani H., Momjian E., Petitjean P., Noterdaeme P., 2013, *MNRAS*, 428, 2198
- Toomre A., 1963, *ApJ*, 138, 385
- Tripp T. M., Lu L., Savage B. D., 1998, *ApJ*, 508, 200
- Wilhelm W., 2013, *Faraday Rotation as a Probe of the Ionised Gas in Distant Galaxies*. Tech. rep., University of Sydney
- Zwaan M. A., Liske J., Péroux C., Murphy M. T., Bouché N., Curran S. J., Biggs A. D., 2015, *MNRAS*, 453, 1268